Nuclear Instruments and Methods in Physics Research A 357 (1995) 110–114

ELSEVIER

NUCLEAR INSTRUMENTS & METHODS IN PHYSICS RESEARCH Section A

The first high resolution, broad band X-ray spectroscopy of ion-surface interactions using a microcalorimeter ☆

Mark LeGros [a], Eric Silver [a,*], Dieter Schneider [b], Joseph McDonald [b], Sophie Bardin [b], Rheinhold Schuch [c], Norman Madden [d], Jeffrey Beeman [d]

[a] *Laboratory for Experimental Astrophysics, Lawrence Livermore National Laboratory, P.O. Box 808, Livermore, CA 94550, USA*
[b] *High Temperature Physics Division, Lawrence Livermore National Laboratory, P.O. Box 808, Livermore, CA 94550, USA*
[c] *University of Stockholm, Vanadisvägen 9, S-113 46, Stockholm, Sweden*
[d] *Lawrence Berkeley Laboratory, 1 Cyclotron Road, Berkeley, CA 94720, USA*

Received 26 October 1994

Abstract

A high resolution, broad band X-ray microcalorimeter has been used for the first time to investigate the radiative deexcitation of highly charged 7 keV/q Ar^{17+} ions as they interact with a beryllium surface at normal incidence. The 20 eV energy resolution of this instrument made it possible to clearly distinguish the argon K_α and $K_{\beta,\gamma}$ complex simultaneously. The intensity ratio of the $K_{\beta,\gamma}$ to K_α emission is 31%, compared to the 8% found in the neutral argon atom. There is strong evidence that the relative intensities of the KL^n ($n = 1$–8) transitions do not agree with those obtained with crystal spectrometers.

1. Introduction

The processes that dictate the neutralization of slow, highly charged ions as they approach and penetrate the surface of a metal have fundamental interest [1,2]. Generally, it is believed that highly charged ions efficiently capture a large number of electrons into high quantum states. The ionic configuration is termed a "hollow atom" – one with virtually an empty core surrounded by electrons occupying high Rydberg levels. The extreme population inversion produced in these ion–surface interactions has the potential to be exploited for X-ray laser schemes if a highly dense plasma could be produced against a metal surface.

The dynamics of the decay of these hollow atoms depend strongly on their velocity. Slow ions generally decay via Auger, X-ray and UV transitions before they reach the first atomic layer of the surface, while fast ions neutralize via bulk interactions beneath the surface. Insights into these mechanisms are obtained from measurements of electron and photon emission spectra as a function of incident ion velocity.

X-ray spectra have been obtained in ion-surface experiments with low resolution ($E/\Delta E \sim 50$) semiconductor ionization detectors for $Ne^{9+,10+}$ [1], $Ar^{17+,18+}$ [3–5], Kr^{36+} [6], $Xe^{44+-48+}$ [7] and $U^{62+-73+}$ [8]. High resolution measurements have been made on Ne^{9+} and $Ar^{17+,18+}$ using crystal spectrometers ($E/\Delta E \sim 500$) [9]. Early experiments were performed by Donets, who bombarded a beryllium target with Ar^{17+} ions with a velocity of 3×10^7 cm/s and measured the X-ray emission with a germanium ionization detector. Similar measurements by Briand et al. were made with a lithium-drifted silicon ionization detector and are shown in Fig. 1. The energy resolution of the detector was not sufficient to separate the contributions of the individual α, β, γ transitions without the use of a spectral model. The entire spectrum covering the Ar $K_{\alpha,\beta,\gamma}$ emission from 2.6 to 4.2 keV was obtained simultaneously.

Briand et al. [4,10] also conducted more detailed studies of the narrow band K_α emission with a crystal spectrometer. Although the crystal spectrometer is rather inefficient, it was capable of resolving the emission from L–K transitions with the number of L electrons ranging from 1 to 8 (see Fig. 2).

Here, we report on the first use of a high resolution, broad band microcalorimeter as an X-ray spectrometer for the study of Ar^{17+} ions interacting with a beryllium target at normal incidence. This experiment took advantage of the ion source capability of the Electron Beam Ion Trap (EBIT) at Lawrence Livermore National Laboratory

☆ This work was performed under the auspices of the U.S Department of Energy by the Lawrence Livermore National Laboratory under the contract No. W-7405-Eng-48.

* Corresponding author. Tel. +1 510 486 4588, fax +1 510 486 4122, e-mail esilver@imager.llnl.gov.

SSDI 0168-9002(94)01469-8

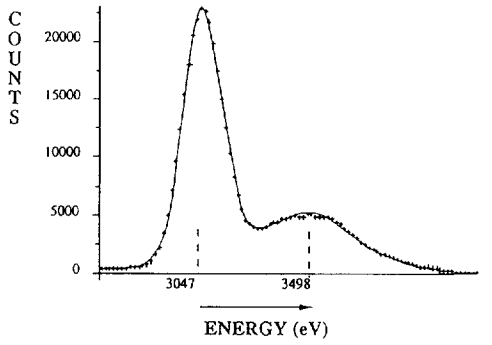

Fig. 1. Ar^{17+} K_α spectrum observed with a lithium-drifted silicon (Si(Li)) detector. The target is silver (Ag) plus carbon (C) (contamination) [4].

(LLNL) to produce these highest charge-state ions [11]. The microcalorimeter not only can measure efficiently the broad energy band covered by the semiconductor ionization detector, but it can simultaneously provide an energy resolution comparable to that of a crystal spectrometer.

2. Microcalorimeter performance

Microcalorimeter development has been motivated, to date, by space-based, high energy X-ray astronomy applications [12,13]. Operating at temperatures between 50 mK and 300 mK, microcalorimeters provide high resolution spectra without the bandwidth and sensitivity limitations of a crystal spectrometer. In a calorimeter X-ray photons are absorbed and thermalized in a detector which is weakly coupled thermally to a cold bath. The resulting rise in the detector's temperature is measured with a thermal sensor, resulting in a signal proportional to the X-ray energy. For the temperature rise to be measurably large the material must possess a very small heat capacity. In an *ideal* microcalorimeter the photon-induced temperature rise must

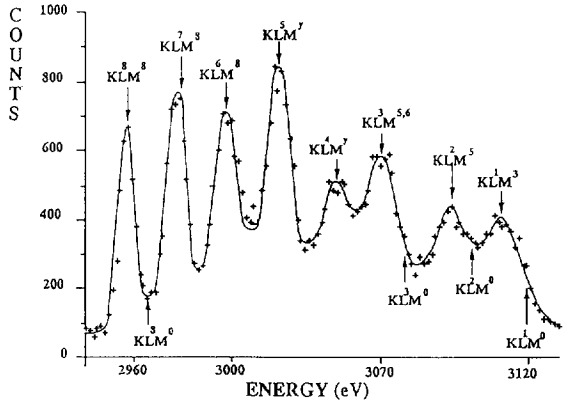

Fig. 2. Ar^{17+} K_α spectrum observed with a flat crystal spectrometer. The target is silver (Ag) plus carbon (C) (contamination) [4].

be measured above background temperature noise caused by the random exchange of energy through the thermal link between the cold stage and the detector. This phonon noise manifests itself in the calorimeter as thermal fluctuations. The mean square value of this thermal noise is $\langle \delta T^2 \rangle = kT^2/C_v$, integrated over all frequencies. If other noise terms are absent, phonon noise would be the only factor limiting the signal to noise ratio, and hence the resolving power, $T/\delta T$. The root mean square energy resolution obtained from this resolving power is $\Delta E = (kT^2 C_v)^{1/2}$. With the proper choice of materials, the resolution of an X-ray calorimeter operating at a temperature of 100 mK, can in principle, be ≤ 1 eV [14]. This resolution is independent of the X-ray energy.

To convert the calorimeter temperature changes into useful voltage signals, experimenters have traditionally taken advantage of the strong temperature dependence of resistance, R, in doped semiconductor crystals [15]. Maximizing the thermistor responsivity, $\alpha = 1/R(\mathrm{d}R/\mathrm{d}T)$, and minimizing the electronic noise will make the best microcalorimeters. Several electronic readout schemes are used and the reader is referred to the literature [14,16].

In practice, the microcalorimeter must be divided into two major components. To maximize the collecting area, the X-rays are absorbed in a high-Z superconductor with very low heat capacity. Since the heat capacity of the doped semiconductor thermistor is the dominant contribution to the device, the thermistor must be made as small as possible and attached to the superconducting absorber. Our recent experiments at 80 mK with NTD (neutron transmutation doped) germanium thermistors coupled to a superconducting absorber of tin demonstrate high spectral resolution (18–20 eV) and high quantum efficiency (95–100%) over the energy band from 0.5 to 7 keV [17].

3. The EBIT and extraction of highly charged ions

The electron Beam Ion Trap (EBIT) is a plasma source that has offered unsurpassed opportunities to measure high resolution X-ray spectra from stationary ions excited by monoenergetic electrons [18]. These spectra have made it possible to measure X-ray transition energies, metastable state lifetimes, and electron-ion collision cross sections for ions of neon to uranium [19].

In the EBIT, neutral gas atoms are multiply ionized by successive collisions with an electron beam. This beam is compressed to ~ 70 μm in a 3-T magnetic field. It not only strips arbitrary elements to any charge state and collisionally populates excited states with high specificity, but it also radially confines the ions. Axial confinement is achieved with an electrostatic potential well created by biasing a segmented axial drift tube assembly [18]. As a consequence, ions are trapped for long time periods enabling precision study of their spectra. At low electron densities ($\sim 10^{12}$ cm^{-3}) the EBIT effectively eliminates

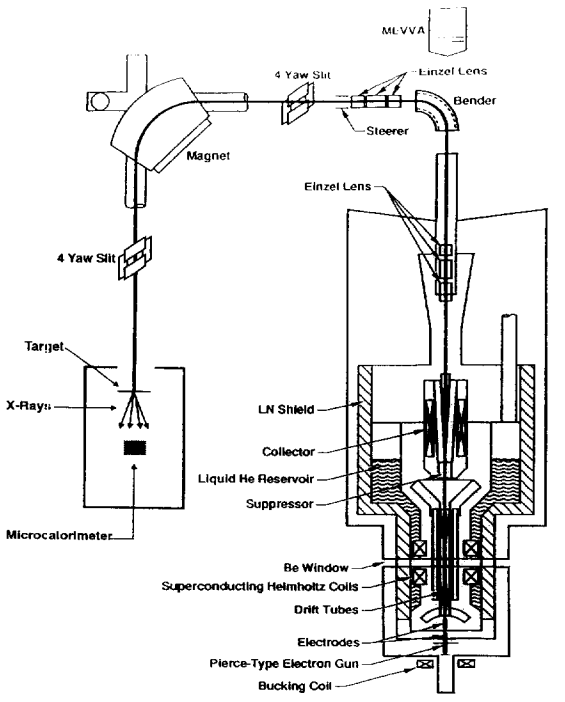

Fig. 3. Schematic of EBIT (Electron Beam Ion Trap) and the ion extraction system [2]. The location of the microcalorimeter cryostat is also indicated.

the transport issues and line-of-sight integrations that compromise the utility of other types of laboratory plasmas (e.g. tokamaks) for studying atomic processes.

All of the ions produced in the EBIT trap can be extracted [11] and transported to a variety of experimental stations. Once equilibrium is reached, the ions are ejected by applying a voltage (~ 7 kV) to one of the outer drift tubes and by raising the middle drift tube potential. These ions are then momentum analyzed and directed through a vacuum beam line toward the target (see Fig. 3).

4. Experimental setup

In the surface physics experiment presented here, the microcalorimeter, discussed in Section 3 [17], was used for the first time to investigate the radiative deexcitation of highly charged 7 keV/q Ar^{17+} ions as they were steered out of the EBIT and into a thin beryllium surface at normal incidence. Fig. 4 schematically shows the internal geometry of the detector and cryostat. The microcalorimeter cryostat was connected to the vacuum beam line in such a way as to allow the highly charged ions to travel into the cryostat where it struck a 25 μm beryllium target. This target was mounted on the end of a collimating tube connected to the 1.8 K (pumped ^{4}He) stage that served as part of a two component thermal radiation shield. The

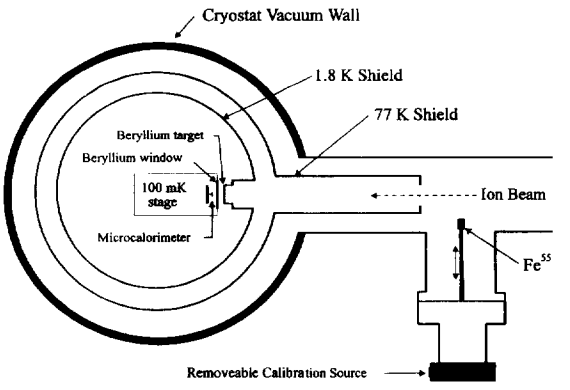

Fig. 4. A schematic view of the internal geometry of the microcalorimeter and cryostat.

second component was an open-ended tube attached to the 77 K (LN_2) stage that extended into the vacuum beam line. These thermal collimators reduced the thermal radiation load on the 0.1 K detector stage to an acceptable level. The microcalorimeter was located in a 0.1 K enclosure that incorporated a 25 μm beryllium window to efficiently transmit the ~ 3 keV Ar K X-rays. A radioactive source of ^{55}Fe was incorporated into the beam line on a linear feedthrough for in-situ calibration of the microcalorimeter at 5.89 keV and 6.49 keV (Mn K_α, K_β). Approximately 10^4 Ar^{17+} ions were extracted from the EBIT during a 100 ms extraction cycle. Since the detector subtended a solid angle at the point of ion impact on the beryllium target of

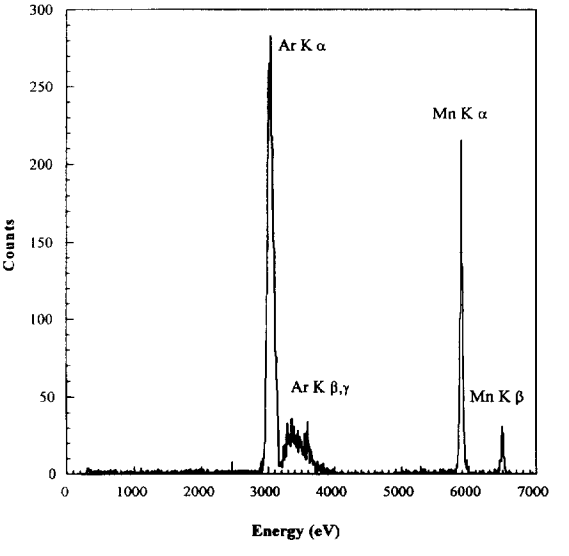

Fig. 5. The microcalorimeter spectrum obtained from Ar^{17+} ions as they struck a 25 μm beryllium target with a velocity of 8×10^7 cm/s. The calibration lines from Mn K_α and Mn K_β, measured in-situ, are also shown.

$\approx 2.5 \times 10^{-3}$ sr, the net count rate on the detector was ~ 2 photons per ion dump.

5. Measurements

Ar^{17+} ions with a velocity of 8×10^7 cm/s struck the 25 μm beryllium target. The microcalorimeter spectrum, including the calibration lines from Mn K_α and Mn K_β, is shown in Fig. 5. Using the Mn K X-rays, we measured the energy resolution of the microcalorimeter to be 20 eV. This resolution is an improvement of at least 7 times over the previous measurements obtained with silicon and germanium ionization detectors at 6 keV. At 3 keV the improvement is at least a factor of 6. This made it possible to clearly and unambiguously distinguish the argon K_α and $K_{\beta,\gamma}$ complex simultaneously, which are shown in an expanded view in Fig. 6. The intensity ratio of the $K_{\beta,\gamma}$ to K_α emission is 31%, compared to the 8% found in the neutral argon atom. The vertical lines in the spectrum represent the energies of the L–K transitions measured previously with a crystal spectrometer with 5–6 eV resolution [4]. The 20 eV resolution of the microcalorimeter just begins to resolve the strong KL^5 and KL^6 components. More importantly, the spectrum indicates that the contributions from transitions KL^5 and KL^6 are the most intense. This is in marked contrast to the measurements made with crystal spectrometers by Briand et al. and the results inferred from the measurements with a germanium ionization detector made by Donets.

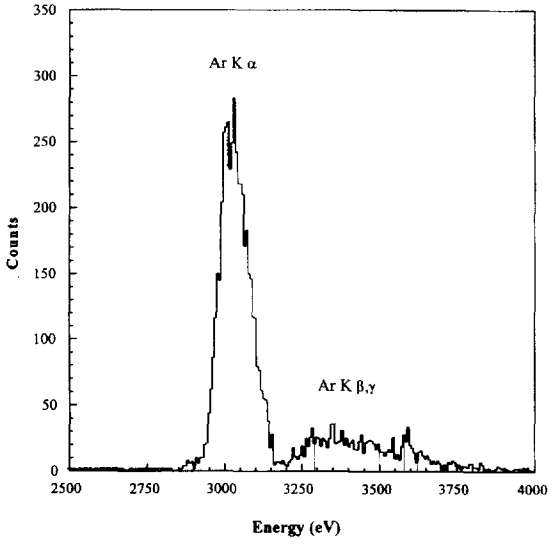

Fig. 6. An expanded view of the Ar K_α and $K_{\beta,\gamma}$ complex. The intensity ratio of the $K_{\beta,\gamma}$ to K_α emission is 31%. The vertical lines represent the energies of the L–K transitions measured previously with a crystal spectrometer with 5–6 eV resolution [4].

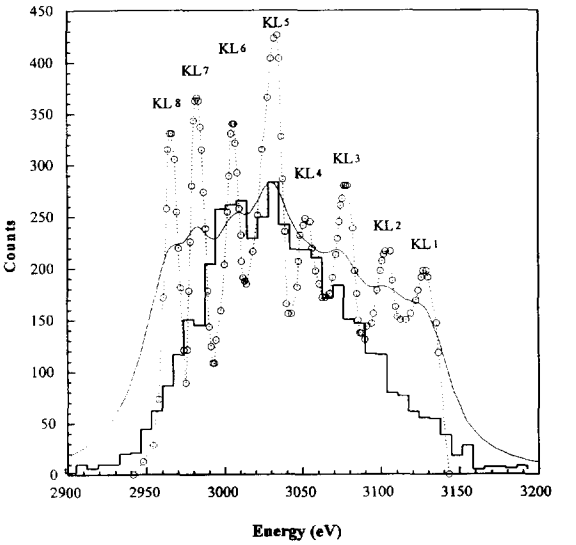

Fig. 7. A comparison of the crystal spectrometer data for Ar K_α from Fig. 2 (dotted) with the microcalorimeter data (solid histogram). The thin, smooth, solid curve represents the convolution of the crystal spectrometer data with the microcalorimeter instrument response function using an energy resolution of 20 eV. The convolved spectrum is normalized so that its peak intensity equals the intensity of the KL^5 transition measured by the microcalorimeter. If the relative intensities of the KL^n transitions were the same for both measurements, the smooth curve would coincide with the microcalorimeter data.

6. Discussion and conclusions

The high resolution of the microcalorimeter made it possible to measure the Ar^{17+} K_α, K_β, and K_γ X-ray spectra simultaneously for the first time. It also enabled us to observe KL^n transitions with relative intensities differing from work performed previously. To compare the overall spectral shapes of the measurements made to date, we have scaled the crystal spectrometer data from Fig. 2, overlayed it on our microcalorimeter data and display them together in Fig. 7. We have also convolved the crystal data with the microcalorimeter instrument response function and depict the result by the smooth solid curve. It is clear that the relative intensities of the KL^n ($n = 1$–8) transitions observed with a crystal spectrometer are very different than those observed with the microcalorimeter. Discussions in the literature of the crystal spectroscopy data state that the intensities of the eight K–L transitions in Ar^{17+} were comparable to within a factor of two, regardless of incident velocity [10]. The crystal spectrometer data reproduced in Fig. 7 are a subset of the experiments done for

varying incident velocities and are consistent with this finding. The data also show that the low and high n states are stronger relative to the $n = 5$ transition than that observed by the microcalorimeter.

The reasons for these discrepancies are not clear at this time. It has been suggested that the KL^n distribution strongly depends on the nature of the target and surface [20]. We note, however, that a crystal spectrometer would have required an ion source 300 times more intense or an observation time 300 times longer to achieve equivalent results on the EBIT. The broad band sensitivy of the microcalorimeter also eliminated the uncertainties associated with cross-calibrating a series of narrow band measurements with one or more Bragg crystal spectrometers. These may be hints to why the measurements are different.

This experiment demonstrated the power of the high resolution, broad band, high efficiency microcalorimeter technique. It showed without a doubt, that this new spectral analyzer can operate in an environment where it was subjected to severe mechanical, acoustic and electromagnetic interference without any degradation in performance. As further progress is made in improving the energy resolution, this instrument promises to be the spectrometer of choice for ion-surface measurements.

Acknowledgements

The authors wish to thank Doren Van Lue and Dan Nelson for their expert technical assistance in conducting these measurements.

References

[1] H.J. Andrä, A. Simionovici, T. Lamy, A. Brenac, G. Lamboley, J.J. Bonnet, A. Fleury, M. Bonnefoy, M. Chassevent, S. Andriamonje and A. Pesnelle, Z. Phys. D 21 (1991) S 135.

[2] D.H. Schneider, M.A. Briere, J. McDonald and J. Biersack, Radiat. and Defects in Solids 127 (1993) 113.

[3] E.D. Donets, Nucl. Instr. and Meth. B 9 (1985) 522.

[4] J.P. Briand, B. d'Etat, D. Schneider, M. Clark and V. Decaux, Nucl. Instr. and Meth. B 87 (1994) 138.

[5] M. Schulz, C.L. Cocke, S. Hagmann, M. Stöckli, H. Schmidt-Böcking, Phys. Rev. A 44 (1991) 1653.

[6] E.D. Donets, S.V. Kartashov and V.P. Ovsyannikov, Proc. Int. Conf. on Phenomena in Ionized Gases, Budapest (1985) p. 228.

[7] M.W. Clark, D. Schneider, D. Dewitt, J.W. McDonald, R. Bruch, U.I. Safranova, I.Y. Tolstikhina and R. Schuch, Phys. Rev. A 47 (1993) 3983.

[8] R. Schuch, D. Schneider, D.A. Knapp, D. DeWitt, J. McDonald, M.H. Chen, M. Clark and R.E. Marrs, Phys. Rev. Lett. 70 (1993) 1073.

[9] J.P. Briand, L. de Billy, P. Charles, S. Essabaa, P. Briand, R. Geller, J.P. Desclaux, S. Bliman and C. Ristori, Phys. Rev. Lett. 65 (1990) 159.

[10] J.P. Briand, AIP Conf. Proc. XVIII ICPEAC, Aarhus, Denmark, 295 (1993) 731.

[11] D. Schneider, M. Clark, B.M. Penetrante, J. McDonald, D. DeWitt and J.N. Bardsley, Phys. Rev. A 44 (1991) 3119.

[12] S. Holt and R. McCray, Ann. Rev. Astron. Astrophys. 20 (1982) 323.

[13] E. Silver, S. Labov, T. Pfafman, Y. Wai, J. Beeman, F. Goulding, D. Landis, N. Madden, and E. Haller, Proc. of Superconducting Tunnel Junctions for X-Ray Detection, Naples (World Scientific, 1990) p. 18.

[14] S.H. Moseley, J.C. Mather and D. McCammon, J. Appl. Phys. 56 (1984) 1257.

[15] E.E. Haller, Infrared Phys. 25 (1985) 257.

[16] E. Silver, S. Labov, F. Goulding, N. Madden, D. Landis, J. Beeman, T. Pfafman, L. Melkonian, I. Millet and Y. Wai, Proc. SPIE 1159 (1989) 423.

[17] M. LeGros, E. Silver, M. Madden, J. Beeman, F. Goulding, D. Landis, and E. Haller, (1994), Nucl. Inst., and Meth. A 345 (1994) 492.

[18] Roscoe E. Marrs, submitted to Meth. Exp. Phys. UCRL-JC-117432, (1994) in press.

[19] P. Beiersdorfer, Nucl. Instr. and Meth. B 56/57 (1991) 1147.

[20] J.P. Briand, private communication (1994).